

Received December 29, 2020, accepted January 7, 2021, date of publication January 11, 2021, date of current version January 22, 2021.

Digital Object Identifier 10.1109/ACCESS.2021.3050795

# Pareto Optimal Allocation of Flexible Fault Current Limiter Based on Multi-Objective Improved Bat Algorithm

ZHENGYU SHU<sup>1,2</sup>, YIQIANG CHEN<sup>3,5</sup>, CHANGHONG DENG<sup>4</sup>,  
FENG ZHENG<sup>3</sup>, AND HAO ZHONG<sup>1,2</sup>

<sup>1</sup>School of Electric and New Energy, Three Gorges University, Yichang 443002, China

<sup>2</sup>Hubei Province Key Laboratory for Operation and Control of Cascade Hydropower Station, China Three Gorges University, Yichang 443002, China

<sup>3</sup>College of Electrical Engineering and Automation, Fuzhou University, Fuzhou 350108, China

<sup>4</sup>College of Electrical Engineering and Automation, Wuhan University, Wuhan 430072, China

<sup>5</sup>State Grid Quanzhou Power Supply Company, Quanzhou 362000, China

Corresponding authors: Feng Zheng (zf@fzu.edu.cn) and Hao Zhong (zhonghao022@163.com)

This work was supported in part by the Natural Science Foundation of Fujian Province, China, under Grant 2019J01249, and in part by the National Key Research and Development Program of China under Grant 2017YFB0902200.


**ABSTRACT** With the sustainable growth in the integration of distributed generation units in the distribution network, the probability of the fault current level exceeding the rating of existing components increases. Cascaded H bridge fault current limiter is widely used in the power grid due to its advantage in inhibiting surge current flexibly. In order to equilibrate the objective functions of its cost, fault current mitigation effect, and the weighted load reliability index, a novel methodology is proposed to simultaneously optimize the location and size of the limiters in the distribution network. Therein, the sensitivity factor considering the Monte Carlo fault simulation model is introduced to reduce the search space and rank candidate locations referencing the actual conditions. And then, according to the candidate locations and considering different conflicting objective functions, a multi-objective improved bat algorithm is employed to obtain the Pareto optimal solution set. Also, life cycle cost and net present value are introduced to construct an economic model to access the scheme costs and service life. The proposed approach is verified using the modified IEEE 33-bus distribution systems with DGs and IEEE 30-bus Benchmark system. The results demonstrate that the proposed method exhibits higher efficiency in finding optimum solutions and provides a new economic configuration idea for the practical engineering application.

**INDEX TERMS** Pareto optimal configuration, cascaded H bridge fault current limiters, sensitivity factor analysis, multi-objective optimization, life cycle cost.

## I. INTRODUCTION

Because of the increasing demand for electricity and continuous growth of distributed generations (DGs), fault current has been larger. In some cases, it may exceed the ratings of existing circuit breakers (CBs), disturb the coordination of protective relays and damage system equipment. Therefore, the excessive short current has become an essential factor affecting the safe and stable operation of Active Distribution Networks (ADNs). As a traditional solution, however, raising voltage grade and installing a high impedance transformer/the series reactor limit the flexibility of ADNs and increase

the network loss [1]. An alternative solution coping with these issues is to employ the fault current limiters (FCLs) such as superconducting fault current limiter (SFCL) and flexible fault current limiter (FFCL) [2]–[4]. In the regular operation of power systems, almost all FCLs exhibit a nearly zero impedance as an invisible device. When a fault occurs, FCLs present a high impedance to limit the short current. However, these approaches have some drawbacks: owing to the heat dissipation problems of SFCL, it cannot be widely used. Although FFCL can flexibly suppress the fault current to the reference value, the withstand voltage and current levels of power electronic devices are still an important factor affecting their development in medium and high voltage distribution networks. With the development of multi-cascaded

The associate editor coordinating the review of this manuscript and approving it for publication was Seifedine Kadry .

converters, cascaded H-bridge current limiters (CHB-FCLs) are widely favored, which can effectively alleviate surge current and are suitable for medium voltage distribution network environment [5], [6].

The limiting current effect of CHB-FCLs is dependent on their number, location, and capacity. And their installation and maintenance costs are as higher as the conventional FCL. To achieve an equilibrium between action efficiency and cost, the location and capacity optimal problems of CHB-FCLs are becoming increasingly important. At present, the solution techniques for their location and capacity optimal problems are attained via traditional mathematical programming methods or intelligent methods. However, with the increase of computational complexity and research scope, the conventional enumeration method cannot find the optimal solution [7]. In [8], an iterative mixed integer nonlinear programming approach is introduced to solve the optimal location and sizing of FCLs in mesh networks, which minimizes the total installed cost. The works, presented in [9], [2], establish an optimal allocation of FCLs for enhancing power system security and stability by using mixed-integer nonlinear programming. However, along with the complexity of the optimal problem increasing, and the shortcomings of complex models, low operating efficiency and poor versatility being revealed, the traditional mathematical programming methods are prevented from being widely used.

In [10], the optimal sizes and locations of FCLs are determined using particle swarm optimization (PSO) to enhance the reliability/economy of the power system and reduce the power loss. A two-stage optimization approach is proposed in [11]. In stage I, a hashing-integrated genetic algorithm is employed to optimize the FCL placement problem. In stage II, the optimal shunt reactance of FCL is determined by PSO. In [12], a fuzzy imperialism competitive algorithm is presented to reconfigure the network and resolve the location and capacity optimal problems of FCLs simultaneously. And its objective functions are to maintain fault current levels and reduce power losses. In [13], a biogeography-based optimization method is used to measure optimal FCL impedance in terms of maximizing the benefit with FCL. Nevertheless, a limitation of the above-listed papers is represented by the fact that they transform a multi-objective problem into a single objective problem by using weight coefficients, which led to the subjectivity and inaccuracy of the FCL's optimal problem.

Along with the objective dimension increasing, multi-objective optimization algorithms exhibit more excellent performance than single-objective optimization algorithm in handling such problems. In [14], the Pareto optimal solution set of resistive-type FCLs are obtained by using an improved multi-objective particle swarm optimization (MOPSO) and a multi-objective artificial bee colony. In [15], a nondominated sorting genetic algorithm (NSGA-II) is applied to optimize the allocation of DGs and FCLs to reduce fault negative effects on distribution networks. Based on the decomposition strategy, a multi-objective evolutionary algorithm is

used to improve the reliability and fault current reduction in [16]. A differential evolution multi-objective algorithm and a complex artificial bee colony algorithm are employed to optimize the allocation of FCLs for minimizing FCL's cost and fault current mitigation in [17], [18]. In order to improve computational efficiency and accuracy, the sensitivity factor is used to pick out the best scheme for active FCL installation in [19]. In [20], the effective/dominated candidate locations are sort out from the search space by sensitivity analysis. Nevertheless, the development of the above algorithms are restricted by the optimal local solution and without adequately considering the cost of the CHB-FCLs.

For making up for the shortage of the above methods, a novel methodology for Pareto optimal allocation of CHB-FCLs is proposed. In the proposed approach, the sensitivity factor analysis method including the Monte Carlo fault simulation model is introduced to simulate fault locations and choose better candidate locations. Among them, the Monte Carlo fault simulation model constructs probability function distribution through the Analytic Hierarchy Process (AHP) and Entropy Weighted Method (EWM), and the random number is used to calculate the probability of fault occurrence. Considering the objectives of the cost, fault mitigation, and Weighted Load Reliability Index (WLRI), a multi-objective improved bat algorithm (MOIBA) is proposed to obtain the Pareto optimal set and compared with MOPSO and NSGA-II. Thereinto, the stochastic inertia weight (SIW) strategy, the iterative local search (ILS) strategy, the balance strategy, and the non-dominant sorting strategy are introduced in MOIBA to overcome the shortcoming of local optimums and premature convergence. Furthermore, Life Cycle Cost (LCC) and Net Present Value (NPV) are introduced to construct the economic evaluation model of CHB-FCLs. This model calculates the actual service life of FCL based on the heat loss fitting and establishes various cost functions. Finally, The results obtained by testing the IEEE 33-bus test system and IEEE 30-bus Benchmark system demonstrate the efficiency of the proposed method.

This study is organized into six sections. Following the Introduction, the mathematical model of CHB-FCL and sensitivity factor analysis are presented in Section II. The formulation of the optimization problem and the procedure of MOIBA are stated in Section III. Section IV constructs the LCC model. The simulation results are discussed in Section V, and the conclusion is given in Section VI.

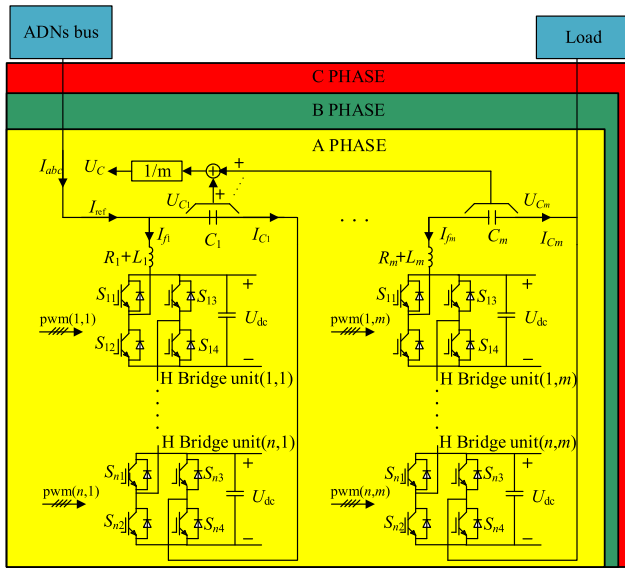
## II. MATHEMATICAL MODEL OF CHB-FCL AND SENSITIVITY FACTOR ANALYSIS

By equating CHB-FCLs to variable impedance, the CHB-FCLs can precisely suppress the current to the target value within the allowed range. In order to speed up the search of the Pareto optimal set, the candidate branches are screened by combining sensitivity analysis and Monte Carlo fault simulation mode [21]–[23].

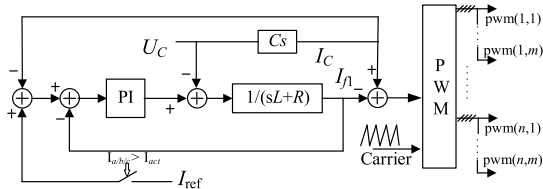
**A. MATHEMATICAL MODEL OF CHB-FCL**

Fig. 1(a) shows a schematic diagram of the CHB-FCL model, which includes the H-bridge units and the series capacitances. Here,  $C_i/L_i/R_i$  ( $i = 1 \dots m$ ) is the capacitance/inductances/resistance of CHB-FCL.  $n$  and  $m$  respectively represent the number of series capacitances and the cascaded H-bridge converter.  $U_{dc}$  is the DC voltage of the H-bridge converter.  $I_{fm}$ ,  $U_{Cm}$ ,  $I_{Cm}$ ,  $I_{ref}$  are inductor current, capacitor voltage, capacitor current and reference current, respectively.  $pwm$  is the modulation wave of the cascaded H bridge.  $S_{ni}$  ( $i = 1 \dots 4$ ) is the switch action variable of the H bridge unit. Because the number of the series capacitances can be conveniently enlarged so as to the withstand voltage capacity of the single series capacitor and cascaded H bridge converters can be significantly enhanced, this structure of CHB-FCL is convenient to expand the capacity of the FCLs.

From Fig 1(b), the main goal of the cascade H bridge converters is through four switchings offering specific current to make CHB-FCL equivalent to a variable impedance. Therefore, when grid system fault happens and the phase current,  $I_{a/b/c}$ , exceeds the trigger current,  $I_{act}$ , CHB-FCLs are triggered to quickly suppressed fault current to its pre-set value.



(a) Scheme diagram of CHB-FCL model



(b) Control block diagram of CHB-FCL

**FIGURE 1. Scheme diagram of the CHB-FCL model and PI control.**

In order to present the current-limiting effect clearly, it is supposed that the symmetrical three line to ground (3LG) fault occurs at 0.1s, the CHB-FCLs are triggered at 0.15s,

the reference current is switched from 2pu to 3pu at 0.3s and the 3LG fault is eliminated at 0.45s.

From Fig. 2, when the fault current exceeds the threshold of the CHB-FCL at 0.1s and where consider 0.05s delay time, the per-unit value of fault current can be limited from 10pu to 2pu at 0.15s. With the change of reference current at 0.3s, the fault current tracks the target value accurately. Therefore, CHB-FCL can effectively limit the fault current to the target value.

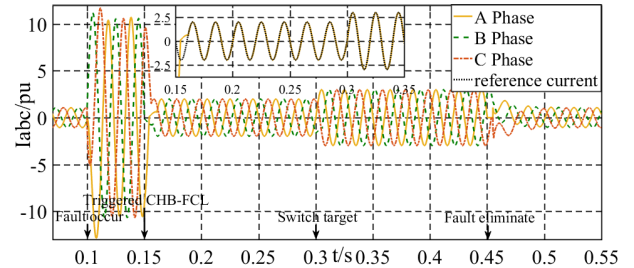


**FIGURE 2. Simulated responses of CHB-FCLs when 3LG fault.**

In addition, the suggested CHB-FCL has the following advantages [21]: (1) Large current limiting inductances are not required. (2) There is no high-frequency oscillation problem. (3) No need to cooperate with solid state circuit breaker. (4) The huge transformer is replaced by the capacitive coupling structure, which not only reduces the cost, but also does not exist excitation inrush current. (5) The topology can be applied to active filtering and other fields, so that the device will not be idle when the line is operating normally. Based on the above factors, CHB-FCL is selected as the planning subject.

According to the principle of substitution and superposition, the fault circuit can be divided into a normal component and a fault component. The voltage equation can be written as follows:

$$\begin{bmatrix} \dot{U}_1 \\ \dots \\ \dot{U}_f \\ \dots \\ \dot{U}_n \end{bmatrix} = \begin{bmatrix} \dot{U}_{1(0)} \\ \dots \\ \dot{U}_{f(0)} \\ \dots \\ \dot{U}_{n(0)} \end{bmatrix} + \begin{bmatrix} Z_{11} & \dots & Z_{1f} & \dots & Z_{1n} \\ \dots & \dots & \dots & \dots & \dots \\ Z_{f1} & \dots & Z_{ff} & \dots & Z_{fn} \\ \dots & \dots & \dots & \dots & \dots \\ Z_{n1} & \dots & Z_{nf} & \dots & Z_{nn} \end{bmatrix} \begin{bmatrix} 0 \\ \dots \\ -\dot{I}_f \\ \dots \\ 0 \end{bmatrix} \quad (1)$$

where  $\dot{U}_i$  ( $i = 1, 2, \dots, n$ ) and  $\dot{U}_{i(0)}$  are the node voltage and nominal voltage, respectively.  $Z_{ij}$  is the branch impedance value between  $i$  bus and  $j$  bus.  $\dot{I}_f$  is the short-circuit current.

According to Fig. 3 and (1), the calculation method of ADNs' short-circuit current integrating with DGs can be expressed as:

$$\dot{I}_k = \frac{\dot{U}_f(0)}{Z_{ff}} = \frac{\dot{U}_f(0)}{Z_1 + \frac{(Z_s + Z_2) \times Z_{DG}}{Z_s + Z_2 + Z_{DG}}} \quad (2)$$

where  $\dot{U}_f(0)$  is the nominal voltage of the fault bus.  $Z_1$  and  $Z_2$  are the line impedance.  $Z_s$  is the Thevenin impedance to the main network,  $Z_{DG}$  is the equivalent impedance of DG.

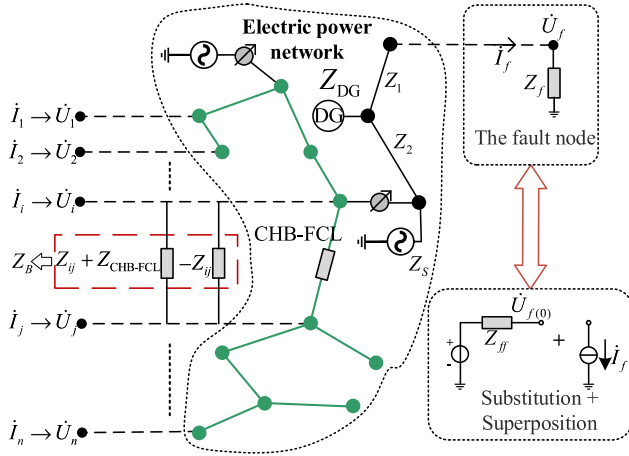


FIGURE 3. Schematic diagram of power network equivalent.

In order to simulate the influence of CHB-FCL in a given network, CHB-FCL impedance is added into the system impedance matrix under fault conditions. Fig. 3 shows that the CHB-FCL is inserted between bus  $i$  and bus  $j$ , which equals to parallel a chain branch with  $Z_B$  in  $ij$  branch. Accordingly, the equivalent impedance  $Z_B$  can be formulated as follows:

$$Z_B = \frac{-Z_{ij}(Z_{CHB-FCL} + Z_{ij})}{Z_{CHB-FCL}} \quad (3)$$

Here,  $Z_{CHB-FCL}$  is the equivalent impedance of CHB-FCL. When CHB-FCL is inserted in the branch  $ij$ , the modified self-impedance  $Z'_{ii}$  is derived as follows [14]:

$$Z'_{ii} = Z_{ii} - \frac{(Z_{ij} - Z_{if})^2}{Z_{ff} + Z_{jj} - 2Z_{ff} + Z_B} \quad (4)$$

### B. SENSITIVITY FACTOR ANALYSIS

For the operation state of a given distribution network, the quantitative relationship between operation variables and control variables can be analyzed by sensitivity. And then the variable's effects on the whole system can be analyzed. The sensitivity factor is defined by the node's self-impedance to reduce the searching range of the objective function and prevent the matrix dimension from being too much. Here, the sensitivity factor,  $\eta_1$ , is

$$\eta_1 = \lim_{Z_{CHB-FCL} \rightarrow 0} \frac{\frac{(Z_{ij} - Z_{if})^2}{Z_{ff} + Z_{jj} - 2Z_{ff} + Z_B}}{Z_{CHB-FCL}} = \frac{(Z_{ij} - Z_{if})^2}{Z_{ff}^2} \quad (5)$$

The traditional sensitivity method calculates the first  $K$  nodes whose short circuit current exceeded the allowable current. And then the branches of the fault nodes are arranged in descending order of sensitivity. The candidate branches are selected from the branches whose sensitivity ranking ahead. However, this method simulates the probability of equal fault and cannot reflect the fault conditions of different nodes in the actual ADNs. Therefore, the Monte Carlo fault simulation

model is introduced in this study, which is a method of calculating the probability occurrence by constructing probability function distribution and using a random number. Thereinto, the line of length ( $X_1$ ), operating life ( $X_2$ ), lightning density ( $X_3$ ), pollution level ( $X_4$ ), and importance ( $X_5$ ) are selected as evaluation indexes to evaluate the combined weight.

### 1) ANALYTIC HIERARCHY PROCESS METHOD

AHP is a hierarchy weight of decision analysis methods to calculate each hierarchy's order. First, making a pairwise importance comparison between the evaluation indexes from  $X_1$  to  $X_5$  and structuring the comparison matrix  $(f_{ij})_{N \times N}$ . Second, calculating the relative weights  $\omega_{AHP}$  and making consistency checks.

$$\omega_{AHP,j} = \frac{1}{N} \sum_{i=1}^N \frac{f_{ij}}{\sum_{k=1}^N f_{ki}} \quad j = 1, 2, \dots, N \quad (6)$$

Here,  $N$  is the dimension of the comparison matrix.

### 2) ENTROPY WEIGHTED METHOD

Based on the difference among the index values, the EWM is proposed. The higher the difference of an index value, the smaller the information entropy. According to the different degree among the indexes, the entropy can be used to calculate each index's weight. There are  $M$  lines and  $N$  indexes.  $(X_{ij})_{M \times N}$  is the original index matrix. The information entropy  $E_j$  is

$$E_j = -\frac{1}{\ln N} \sum_{i=1}^N \left( \frac{X_{ij}}{\sum_{i=1}^N X_{ij}} \ln \frac{X_{ij}}{\sum_{i=1}^N X_{ij}} \right) \quad (7)$$

The weight coefficient  $\omega_{EWM}$  is determined by entropy and it can be expressed as:

$$\omega_{EWM,j} = \frac{1 - E_j}{M - \sum_{j=1}^N E_j} \quad (8)$$

### 3) MONTE CARLO FAULT SIMULATION MODEL

Based on AHP and EWM, the combination weighting method has the advantages of reducing the subjective randomness of weighting and taking into account the decision maker's preference for attributes [24], [25]. The combined weight  $\omega_j$  is expressed as follows:

$$\omega_j = \frac{\omega_{AHP,j} \omega_{EWM,j}}{\sum_{k=1}^N \omega_{AHP,k} \omega_{EWM,k}} \quad j = 1, 2, \dots, N \quad (9)$$

The probability of line failure  $P_i$  can be derived as follows:

$$P_i = \frac{\sum_{j=1}^N \omega_j X_{ij}}{\sum_{i=1}^M \sum_{j=1}^N \omega_j X_{ij}} \quad i = 1, 2, \dots, M \quad (10)$$

According to the probability of fault, the probability density model is represented by the random number,  $k_1$ , which can be expressed as follows:

$$f = \begin{cases} 1 & k_1 < P_1 \\ 2 & P_1 \leq k_1 \leq \sum_{i=1}^2 P_i \\ \vdots & \vdots \\ M & \sum_{i=1}^{M-1} P_i \leq k_1 \leq 1 \end{cases} \quad (11)$$

where  $k_1$  is a random value within  $[0,1]$ .  $f$  is the fault node. Through Monte Carlo's fault simulation point and sensitivity, the total sensitivity of each branch can be calculated. If the value of the sensitivity factor is larger, it means that more effective for mitigating fault and a better current limiting performance can be obtained, installing the CHB-FCL into a branch. And the novel sensitivity factor is

$$\eta = \sum_{i=1}^{t_{\text{fault}}} \frac{(Z_{ij} - Z_{if(k_1(i))})^2}{Z_{f(k_1(i))}^2} \quad (12)$$

where  $t_{\text{fault}}$  is the maximum number of failures.  $f(k_1(i))$  is the fault node at  $i$  times. According to (12), the branches can be screened to be the best candidate locations when the largest sensitivity factor is obtained.

### III. PROPOSED CHB-FCL OPTIMAL ALLOCATION METHOD

#### A. PROBLEM FORMULATION

Considering the cost, mitigation fault effect, and WLRI, this paper proposes a Pareto optimal allocation method for CHB-FCLs. The optimal allocation problem in this method can be regarded as a multi-objective function that is subject to equality and inequality constraints. And it can be formulated by the mathematical equation as follows:

$$\begin{cases} \min F(x) = (\min F_1(x), \min F_2(x), \min F_3(x)) \\ \text{s.t.} \begin{cases} Z_{\text{CHB-FCL}}^{\min} \leq Z_{\text{CHB-FCL}} \leq Z_{\text{CHB-FCL}}^{\max} \\ N_{\text{CHB-FCL}}^{\min} \leq N_{\text{CHB-FCL}} \leq N_{\text{CHB-FCL}}^{\max} \end{cases} \end{cases} \quad (13)$$

where  $x = (x_1, x_2, \dots, x_n)$  represents the solution to the three-dimensional problem.  $F(x)$  is the target space of the three-dimensional problem.  $N_{\text{CHB-FCL}}$  is the number of CHB-FCL.  $Z_{\text{CHB-FCL}}(i)$  is the impedance of CHB-FCL. From (13), the Pareto optimal solution is a solution set, and it is limited by objective functions and constraint conditions.

The first objective function,  $F_1$ , for optimal allocation of CHB-FCLs is to minimize the capital cost of the CHB-FCLs. The cost of the current limiter includes installation cost and capacity cost. And installation cost is proportional to the number of CHB-FCLs. The capacity cost is significantly correlated with the impedance value of the CHB-FCLs. Therefore, it is necessary to choose the configuration scheme with the least number of installation stations and the least capacity.

Accordingly, the first objective function can be expressed as

$$F_1 = N_{\text{CHB-FCL}} + \sum_{i=1}^{N_{\text{CHB-FCL}}} Z_{\text{CHB-FCL}}(i) \quad (14)$$

The second objective function,  $F_2$ , is used to evaluate the current-limiting ability of the CHB-FCL [14]. And it is

$$F_2 = \log_M \left[ \sum_{i=1}^M f_{\text{rate}} \left( \frac{I_{\text{CHB-FCL}}(i)}{I_{\text{without}}(i)} \right) \right] + f_{\text{pena}} \quad (15)$$

$$f_{\text{pena}} = \frac{p_c \sum_{i=1}^M \max \{ I_{\text{CHB-FCL}}(i) - I_{\text{per}}^{\max}, 0 \}}{\sum_{i=1}^M I_{\text{without}}(i)} \quad (16)$$

$$f_{\text{rate}}(a) = \begin{cases} (M+1)^{k-1}, & \frac{k-1}{s} \leq a \leq \frac{k}{s} \quad (k=1, 2, \dots, s) \\ (M+1)^s, & a \geq 1 \end{cases} \quad (17)$$

where  $I_{\text{CHB-FCL}}(i)$  is the current in  $i$  bus with accessing CHB-FCL.  $I_{\text{without}}(i)$  is the current in  $i$  bus without accessing CHB-FCL.  $f_{\text{pena}}$  is the penalty function and determined by the fault current constraints.  $s$  is the pre-set phase of limiting current proportion.  $p_c$  is a penalty coefficient.  $I_{\text{per}}^{\max}$  is the permissible limit current.  $M$  is the branch of the system. Suppose  $I_{\text{CHB-FCL}}(i)$  is lower than  $I_{\text{per}}^{\max}$ ,  $f_{\text{pena}}$  equals to 0. Otherwise, (17) is achieved. When the difference between the short-circuit current value with and without CHB-FCL is large, the allocation scheme with CHB-FCLs has a better current-limiting effect and lower value of  $F_2$ .

The third objective function,  $F_3$ , is used to evaluate the reliability of ADNs [26]. WLRI is used to estimate the system reliability, which is composed of System Average Interruption Duration Index (SAIDI), Average Service Unavailability Index (ASUI), and Average Energy Not Supplied (AENS). The lower value of WLRI indicates a higher value for system reliability. Accordingly,  $F_3$  can be expressed as

$$F_3 = \sum_{i=1}^M \omega_{\text{CIC},k} \left( \text{WLRI}_{x,i}^{\text{without}} - \text{WLRI}_{x,i}^{\text{CHB-FCL}} \right) \quad (18)$$

$$\begin{aligned} \text{WLRI}_{x,i}^{\text{CHB-FCL}} &= \text{SAIDI}_{x,i}^{\text{FCL}} + \text{ASUI}_{x,i}^{\text{FCL}} + \text{AENS}_{x,i}^{\text{FCL}} \\ &= \frac{\lambda_i^{\text{FCL}} N_i}{\sum_{k=1}^M N_k} + \frac{r_i^{\text{FCL}} \lambda_i^{\text{FCL}} N_i}{8760 \sum_{k=1}^M N_k} + \frac{r_i^{\text{FCL}} P_i}{\sum_{k=1}^M N_k} \end{aligned} \quad (19)$$

$$\lambda_i^{\text{FCL}} = \lambda_i^{\text{without}} - \eta_i^{\text{FCL}} \lambda_{i,\text{faultcurrent}}^{\text{without}} \quad (20)$$

$$\omega_{\text{CIC},k} = \frac{\text{CIC of } i\text{th load point}}{\text{average CIC of all types of customers}} \quad (21)$$

where  $\omega_{\text{CIC},k}$  is the significance of the  $k$ th load and determined by considering customer interruption cost of each customer.  $\lambda_i^{\text{FCL}}$  and  $\lambda_i^{\text{without}}$  are the failure rate of the protective device with CHB-FCL and without CHB-FCL.  $\eta_i^{\text{FCL}}$  is

the fault current reduction efficiency when CHB-FCL is installed.  $N_i$ ,  $r_i^{FCL}$ , and  $P_i$  are the number of customers, repair time, and amount of electric demand power, respectively. A higher index of  $F_3$  means a more suitable place to install CHB-FCL from the viewpoint of reliability improvement.

**B. STANDARD BAT ALGORITHM**

Because microbats continually adjust the searching frequency to update the location of the population, they can avoid obstacles or find prey during their flights [27], [28]. Based on this phenomenon, the bat algorithm (BA), as a meta-heuristic optimization algorithm, is proposed. Hereon, the frequency,  $fr_i$ , speed  $v_i$ , and position  $p_i$  of the  $i$ th virtual microbat are defined as (22), (23), and (24).

$$fr_i = fr_{min} + \tau_1 * (fr_{max} - fr_{min}) \tag{22}$$

$$v_i(t) = v_i(t - 1) + fr_i * (p_i(t - 1) - p_{best}) \tag{23}$$

$$p_i(t) = p_i(t - 1) + v_i(t) \tag{24}$$

where  $fr_i$  is restricted within  $[fr_{min}, fr_{max}]$ .  $\tau_1$  ( $\tau_1 \in (0,1)$ ) is a random number.  $p_{best}$  indicates the current optimum individual.

The local searching operation, as a dominance strategy, is mainly to find a better scheme  $p_{bet}$  near the  $p_{best}$  one by updating the loudness  $lo_i$  and pulse rate  $r_i$ . The update formulas of  $lo_i$  and  $r_i$  are defined as follows:

$$lo_i(t + 1) = \tau_2 lo_i(t) \tag{25}$$

$$r_i(t + 1) = r_0(1 - \exp(-\tau_3 t)) \tag{26}$$

where  $\tau_2$  ( $\tau_2 \in (0,1)$ ) and  $\tau_3$  ( $\tau_3 > 0$ ) represent the attenuation coefficient of  $lo$  and the increase coefficient of  $r$ , respectively.  $r_0$  is the initial pulse rate. After finding prey,  $lo$  is decreased, and  $r$  is increased to improve the searching efficiency.

**C. MOIBA ALGORITHM**

In order to handle the multi-objective optimization problems more effectively, the MOIBA algorithm is introduced, which overcomes the shortcomings of local optimums and premature-convergence and has significant advantages on optimization accuracy and convergence stability [29].

**1) STOCHASTIC INERTIA WEIGHT STRATEGY**

The SIW  $\omega_{SIW}$  is introduced to enhance the convergence of rapidity and precision, which can improve the updating manner of  $v_i$ . The updated formulas of  $v_i$  and  $\omega_{SIW}$  are defined as follows:

$$v_i(t) = \omega_{SIW} v_i(t - 1) + fr_i * (p_i(t - 1) - p_{best}) \tag{27}$$

$$\omega_{SIW} = u_{SIW}^{min} + \tau_4(u_{SIW}^{max} - u_{SIW}^{min}) + \tau_5 \sigma_{SIW} \tag{28}$$

where  $u_{SIW}^{max}$  and  $u_{SIW}^{min}$  are the maximum and minimum influencing factors of SIW.  $\tau_4/\tau_5$  ( $\tau_i \in (0,1)$ ,  $i = 4, 5$ ) is a random number.  $\sigma_{SIW}$  is the deviation coefficient.

**2) ITERATIVE LOCAL SEARCH STRATEGY**

The ILS strategy can obtain the global optimal  $x_*$  when the acceptance criteria are satisfied, which is put forward to jump

out of the local optimal. Here, the update of  $x_*$  is defined as follows:

$$x_* = \begin{cases} x_*' = x_* \tau_6 \\ \text{when } F(x_*') < F(x_*) \text{ or } e^{-(F(x_*') - F(x_*)) > \tau_7} \end{cases} \tag{29}$$

where  $x_*'$  is the intermediate state,  $\tau_6/\tau_7$  ( $\tau_i \in (0,1)$ ,  $i = 6, 7$ ) is a random number. The acceptance criterion is a greedy method with random factors, which guides the search for finding  $p_{bet}$ .

**3) BALANCE STRATEGY**

The balance strategy controls the movements of the bats by  $r_i$  and the acceptance of a new solution by  $lo_i$ , which is applied to balance between local and global search. The renewed manners of  $r_i$  and  $lo_i$  are defined as follows:

$$r_i(t + 1) = \tau_r * r_i(t)^2 * \sin(\pi r_i(t)) \tag{30}$$

$$lo_i(t + 1) = \left( \frac{lo_{max} - lo_{min}}{t - t_{max}} \right) (1 - t_{max}) + lo_{min} \tag{31}$$

where  $\tau_r$  is the iteration parameter.  $lo_{min}$  and  $lo_{max}$  is the limited range of loudness.  $t_{max}$  is the maximum iteration. From Fig.4, it can be seen that the sine map function of  $r_i$  and monotone random filling model function  $lo_i$  exhibit better chaos ergodicity in searching space.

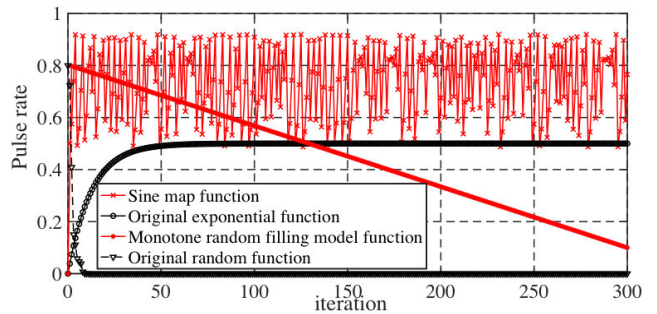


**FIGURE 4. Pulse rate functions and loudness functions.**

**4) NON-DOMINANT SORTING STRATEGY**

In multi-objective optimization, it is impossible to find a solution to minimize all objectives simultaneously due to the conflict's objective functions. The Pareto-optimality, as an essential concept of game theory, is taken into account and states that a non-dominate policy has the property which regardless of how the process entered a given state, the remaining decision must belong to a non-dominated sub-policy [30]. A non-dominated solution  $x_{(1)}$  dominates another solution  $x_{(2)}$  and it can be noted as  $x_{(1)} < x_{(2)}$ .

If and only if:

$$(F_i(x_{(1)}) \leq F_i(x_{(2)}), \quad \forall i) \wedge (F_i(x_{(1)}) < F_i(x_{(2)}), \exists i) \tag{32}$$

After the dominance relationships between individuals are determined, a non-dominant sorting strategy is used to divide the population into different ranks according to the dominance relationships. The non-dominant solution can be

defined as a new rank by traversing the population. And the above procedures are repeated to search the remaining population until all individuals are defined.

Crowding distance is introduced to characterize the distance between individuals, so that the distribution of individuals is more uniform in space. A novel crowding distance  $D(x)$  can be formulated as follows:

$$E(x) = \sum_{i=1}^3 \frac{|F_i(x+1) - F_i(x-1)|}{F_{i,max} - F_{i,min}} \quad (33)$$

$$D(x) = \frac{\sum_{j=2}^{n-1} \left( \left| \sum_{i=1}^3 \frac{|F_i(j+1) - F_i(j-1)|}{F_{i,max} - F_{i,min}} \right| - E(x) \right)^2}{n-1} \quad (34)$$

where  $n$  is the number of populations. Traditional crowding distance  $E(x)$  tends to fail to retain excellent individuals due to the large numerical differences in different dimensions. Therefore the crowding degree variance calculation  $D(x)$  is used to ensure the uniformity of the particle distribution and unlikely to fall into a local solution. Fig. 5 shows the Pareto front set can be obtained by the optimal process of MOIBA. When the number of iterations is  $t_{max}$ , the algorithm stops iteration.

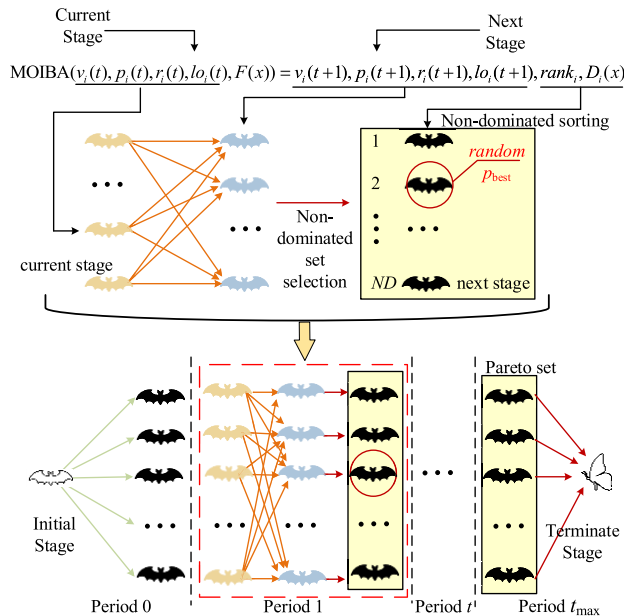


FIGURE 5. The process of MOIBA in multi-objective optimization.

#### D. ALGORITHM PERFORMANCE ANALYSIS

In order to evaluate the convergence and uniformity of the Pareto front solution, the inverted generational distance (IGD) is used as the performance evaluation index [31]. The lower the index value, the better the convergence and diversity of the Pareto front solution obtained by the algorithm, and the closer to the reference Pareto front solution.

The IGD can be expressed as follows:

$$IGD = \frac{1}{|P|} \sum_{i=1}^{|P|} \min_{j=1}^{|A|} \sqrt{\sum_{m=1}^M \left( \frac{f_m(p_i) - f_m(a_j)}{f_m^{max} - f_m^{min}} \right)^2} \quad (35)$$

where  $A$  denotes the nondominated solutions generated by the algorithm.  $a_j \in A, j = 1, 2, \dots, |A|$ .  $P$  denotes a set of reference points in the calculation of IGD.  $p_i \in P, i = 1, 2, \dots, |P|$ .  $f_m^{max}$  and  $f_m^{min}$  are the maximum and minimum values on the  $m$ th target in  $P, m = 1, 2, \dots, M$ .  $M$  is the number of targets.

Table 1 shows the experimental results in terms of IGD between the three multi-objective algorithms on four test instances. The mean value and standard deviation value of IGD are the statistical results of the same algorithm running independently for 50 times on the same test instance [32]. It can be seen that the MOIBA algorithm obtains the minimum mean value and Std. value in a different test instance. And the results show that the MOIBA algorithm has better convergence and uniformity than the traditional multi-objective optimization algorithm (such as NSGA-II and MOPSO). In this section, we only take ZDT1, ZDT2, ZDT3, and ZDT6 as examples. It's important to note that according to the No Free Lunch (NFL) Theorem, we cannot expect the algorithm to get the best IGD value for every test function.

TABLE 1. The IGD value between different algorithms on four test instances.

Test instance		MOIBA	NSGA-II	MOPSO
ZDT1	Mean	1.9E-03	5.1E-01	1.3E-02
	Std.	2.9E-03	7.4E-02	1.8E-03
ZDT2	Mean	3.4E-03	7.6E-01	1.8E-02
	Std.	5.4E-03	1.4E-01	5.1E-03
ZDT3	Mean	9.8E-04	3.6E-01	1.1E-01
	Std.	1.7E-03	4.0E-02	7.1E-02
ZDT6	Mean	1.9E-02	1.65	4.4E-01
	Std.	1.5E-2	9.8E-01	2.4E-02

#### IV. LIFE CYCLE COST MODEL OF CHB-FCL

The economy is one of the critical factors that determine whether an emerging technology can be popularized and applied [33]. According to the IEEE Std. 24748, the LCC criterion is used to calculate the equipment costs comprehensively, which can be expressed as follows:

$$LCC = CI + CO + CF + CD \quad (36)$$

where  $CI$  is the investment cost.  $CO$  is the operation cost.  $CF$  is the maintenance cost.  $CD$  is the disposal cost. The traditional planning problems only aim at equivalenting the research phase and service life, and it does not take into account the replacement of equipment. Consequently, the research phase  $t_r$  is set to be longer than the service life of the equipment  $t_{FCL}$  in this paper, and after the last replacement of the equipment, the residual value of the equipment is

considered in this paper. Based on the replacement, the model of LCC is shown in Fig. 6.

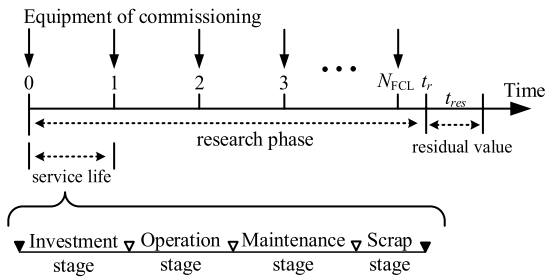


FIGURE 6. The model of LCC is based on equipment replacement.

**A. CHB-FCL SERVICE LIFE**

When the current flowing through the CHB-FCL reaches a particular value, the impact on CHB-FCL’s life cannot be ignored. In [34], the effect of cyclic junction temperature variations of the power electronics module aging process is researched, and it is found that such minor stress cycles contribute to the development of damage and tend to accelerate the end of life. In [35], [36], the thermal stresses can accumulate as fatigue on the devices and challenge the lifetime. Thus, we can know from the above description that the temperature stress has a great influence on the module life of power device. However, the existing research rarely conducts experiments on the quantitative loss of CHB-FCL’s life which is produced by the fault surge current. In this case, the rated life of the equipment cannot reflect the actual life of the CHB-FCL and increases the error of the CHB-FCL cost model.

The wastage of power electronic devices is related to the joule heat generated by the current flowing. Take the thyristor for example. The rated current of the thyristor is limited based on the junction temperature caused by the power dissipation and heating. When the current is less than the effective value (1.57 times the rated current), its heating temperature rise is within the allowable value, and its loss coefficient is close to a small number. It is considered that the device operates indefinitely with the rated service life. When the current exceeds the effective value, the loss coefficient increases correspondingly. When the current exceeds the inrush current, the power electronic device will be directly damaged by the breakdown. As shown in Fig.7, in order to make a preliminary quantitative analysis of the cost of CHB-FCL, a simplified CHB-FCL life loss model is constructed by combing the fatigue life characteristics and the heat loss [27]. If  $I$  is less than the action threshold  $I_{act}$ , there has no loss. If  $I$  is within  $[I_{act}, I_{per}^{max}]$ , a small loss coefficient  $s_{Qmin}$  can be obtained. If  $I$  is within  $[I_{per}^{max}, I_{max}]$  ( $I_{max}$  is the maximum bearing current), due to the law of dissipation is unknown, the quadratic curve function is adopted. Thus, the life decay of FCL will be nonlinear accelerated with the increase of current.

The lifetime loss of CHB-FCL is accumulated by combining the fault points of Monte Carlo simulation, which can be

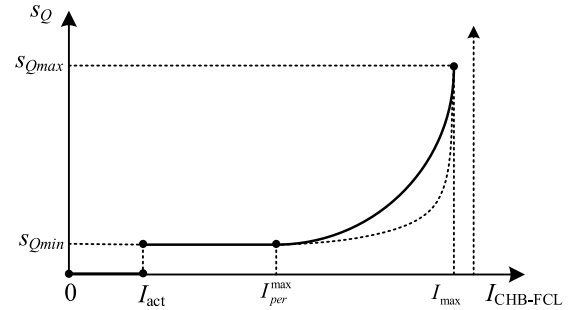


FIGURE 7. The fitting relationship between loss coefficient and current.

formulated as follows.

$$S_{Qsum} = \sum_{k=1}^{t_{fault}} s_Q I_{CHB-FCL,k}^2 Z_{CHB-FCL} T_Q \tag{37}$$

$$\eta_{loss} = \frac{S_{Qsum}}{S_F} \tag{38}$$

where  $T_Q$  is the fault time.  $s_Q$  is the loss coefficient.  $\eta_{loss}$  is the loss ratio.  $S_F$  is the ultimate life. If  $\eta_{loss} = 1$ , it denotes that the corresponding life is the equipment’s  $t_{FCL}$ . It should be noted that the established simplified life loss model of CHB-FCL is used for the preliminary quantitative analysis of the cost model. Once a more accurate CHB-FCL life model is available in the future, it can be directly replaced.

**B. COST STRUCTURE**

Since the research phase is longer than the service life of the equipment, there is some residual value after the last replacement of the equipment in the research phase, so the value outside the research phase should be deducted when calculating the investment cost. The investment cost can be classified into capacity cost and installation cost, which can be expressed as:

$$CI = c_p \left[ \sum_{i=0}^{N_{CHB-FCL}} (npv)^{it_{FCL}} - \left(\frac{t_{res}}{t_{FCL}}\right) (npv)^{t_r} \right] \times \sum_{i=0}^{N_{CHB-FCL}} Z_i^{CHB-FCL} + N_{FCL} c_r \sum_{i=0}^{N_{FCL}} (npv)^{it_{FCL}} \tag{39}$$

$$npv = (1 - q) \left( \frac{1 + b}{1 + p} \right) \tag{40}$$

where  $c_p$  is the capacity cost factor.  $t_{res}$  is the time of residual value.  $c_r$  is the installation costs factor.  $t_r$  is the research phase.  $t_{FCL}$  is the service life of the equipment.  $npv$  is the net present value function.  $q$  is the coefficient of price change.  $b$  is the rate of inflation.  $p$  is the interest rate.

The operation cost includes the input of labor and capital. To simplify the calculation, this paper converts all relevant operating costs into operation cost factor  $k_{co}$ .

$$CO = c_p k_{co} \left( \sum_{i=0}^{t_r} (npv)^i \right) \sum_{i=0}^{N_{CHB-FCL}} Z_i^{CHB-FCL} \tag{41}$$



In order to restore the working capacity of the FCL or to ensure the efficiency of the FCL, the maintenance cost must be considered. And the annual maintenance cost is generally accrued as a percentage of the equipment price in that year ( $k_{cf}$ ). Therefore,  $CF$  can be obtained from the bathtub curve:

$$CF = c_p k_{cf} \left( \sum_{i=0}^{t_r} h_{cf}(i) (npv)^i \right) \sum_{i=0}^{N_{CHB-FCL}} Z_i^{CHB-FCL} \quad (42)$$

where  $k_{cf}$  is the annual maintenance cost factor.  $h_{cf}$  is the hazard rate, which can be obtained by (42) and Fig. 8.

$$h_{cf}(t) = \begin{cases} \alpha_1 - t^{\beta_1-1} & t < t_1 \\ \alpha_2 t^{\beta_2-1} & t > t_2 \end{cases} \quad (43)$$

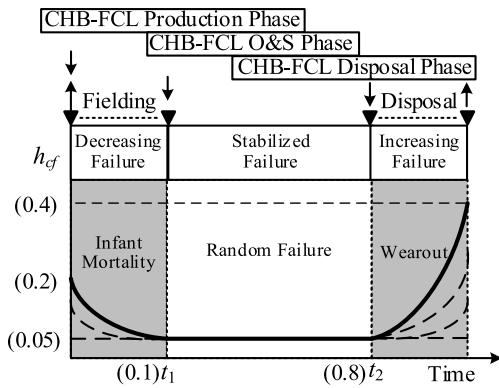


FIGURE 8. The bathtub failure rate curve of CHB-FCL.

where  $\alpha_1$ ,  $\alpha_2$ , and  $\beta_1$ ,  $\beta_2$  are the failure rate function parameters of Weibull distribution, respectively. If  $t$  is less than  $0.1t_{FCL}$ , the failure rate of FCL decreases continuously during Infant Mortality. If  $t$  is within  $[0.1t_{FCL}, 0.8t_{FCL}]$ , the failure rate of FCL is lower and more stable under the Random Failures. If  $t$  is greater than  $0.8t_{FCL}$ , due to aging, wear and other reasons, the failure rate of FCL increase rapidly during the Wearout.

In order to simplify the calculation of the disposal cost of FCL, this paper introduces the disposal cost factor  $k_{cd}$ . The disposal cost can be formulated as:

$$CD = c_p k_{cd} \left( \sum_{i=1}^{N_{CHB-FCL}} (npv)^{it_{FCL}} \right) \sum_{i=0}^{N_{CHB-FCL}} Z_i^{CHB-FCL} \quad (44)$$

## V. SIMULATION AND RESULTS

This section is devoted to verifying the optimal allocation method of the CHB-FCLs in the IEEE 33-bus system and IEEE 30-bus Benchmark system. Considering the increasing demand for power consumption because of the country's economic expansion, it's necessary to plan for additional DGs.

### A. IEEE 33-BUS SYSTEM WITH DGs

Fig. 9 shows the IEEE 33-bus system and Table 2 gives the simulation parameters. The base voltage of the

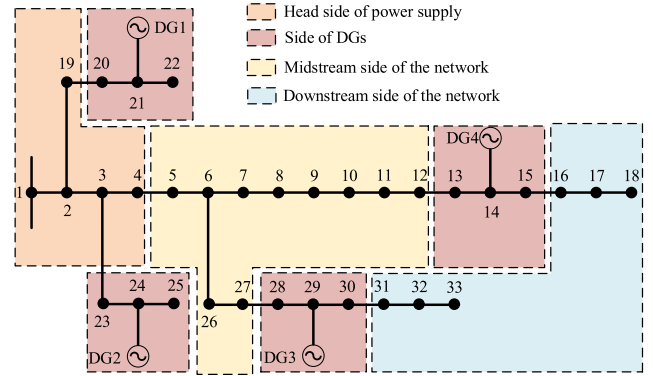


FIGURE 9. Schematic of the modified IEEE 33-bus system with DGs.

ADN is 12.66kV. The total network load is 5084.26 + j2547.32 kVA. Combining [14] and system load capacity, four 500kVA photovoltaic plants (marked as DG1, DG2, DG3, and DG4) are installed at bus 14, 21, 24, and 29, respectively. And the subtransient reactance  $Z_{DG}$  is 0.2.

### 1) SELECTING CANDIDATE LOCATIONS

In the traditional sensitivity analysis model, the nodes whose three-phase short-circuit fault current exceeds 10kA are selected, and the corresponding sensitivity values  $\eta_1$  of all branches under each node are calculated by (5). From Table 3, five fault current nodes and their candidate branches are given. By selecting the repetitive locations and sorting the locations at the front, CHB-FCLs are installed in eight candidate branches, namely, 19-20, 20-21, 3-23, 24-25, 6-26, 30-31, 31-32, and 32-33. However, the traditional sensitivity analysis model does not consider the actual situation of the distribution network, which leads to unnecessary planning, such as continuous placement of adjacent lines and failure to consider the importance of branches.

In the proposed sensitivity factor analysis, the Monte Carlo fault simulation is set as 1500 times, the equivalent duration of the simulation is 15 years. Through the parameters of  $X_1$  to  $X_5$  in Table 2, the fault probability model of each line is established by calculating the weight of AHP ( $\omega_{AHP} = [0.0526, 0.1053, 0.2105, 0.2105, 0.4211]$ ) and the weight of EWM ( $\omega_{EWM} = [0.2157, 0.2977, 0.1812, 0.1153, 0.1901]$ ). The probability of line failure can be obtained through (9, 10), and is listed in  $[P_1, P_2]$  in Table 2. Then, the candidate positions of the fault current limiter are sorted by calculating the sensitivity value  $\eta$ .

It can be seen from Table 4, the top eight branches of the total value of sensitivity factors are selected as candidate locations. The proposed method accumulates all the sensitive factors of the branches based on the Monte Carlo fault simulation points, and the results not only take into account the actual situation of the network but also significantly reduce the invalid search range of the multi-objective optimization algorithm.

TABLE 2. The simulation parameters of the fault line model and customer data in IEEE 33-bus system.

From <i>i</i>	To <i>j</i>	Branch impedance (Ω)	Load of <i>j</i> (kVA)	X <sub>1</sub>	X <sub>2</sub>	X <sub>3</sub>	X <sub>4</sub>	X <sub>5</sub>	Type	Number of Customers	$\omega_k$	[ <i>P</i> <sub>1</sub> , <i>P</i> <sub>2</sub> ]
1	2	0.0922+j0.047	100+j60	30	30	4.5	3.9	10	Large user	1	1.8	[0,0.07]
2	3	0.4930+j0.2511	90+j40	10	300	4.4	3.9	7	Large user	1	1.7	[0.07,0.13]
3	4	0.3660+j0.1864	120+j80	9	25	4.1	3.2	4.5	Large user	1	1.6	[0.13,0.17]
4	5	0.3811+j0.1941	60+j30	8	27	4.0	3.5	4	Large user	1	1.4	[0.17,0.21]
5	6	0.8190+j0.7070	60+j20	12	25	3.2	3.1	3.8	Small user	1	1.4	[0.21,0.25]
6	7	0.1872+j0.6188	200+j100	13	25	2.7	3.0	3.5	Residential	220	0.5	[0.25,0.28]
7	8	0.7114+j0.2351	200+j100	3	25	2.5	0.8	3.2	Residential	220	0.5	[0.28,0.30]
8	9	1.0300+j0.7400	60+j20	6	23	2.8	2.5	3.1	Commercial	10	1.5	[0.30,0.32]
9	10	1.0440+j0.7400	60+j20	14	23	3.0	1.3	3.0	Commercial	10	1.5	[0.32,0.35]
10	11	0.1966+j0.0650	45+j30	17	22	2.6	2.6	3	Commercial	10	1.5	[0.35,0.37]
11	12	0.3744+j0.1238	60+j35	11	22	2.3	2.0	3	Commercial	10	1.5	[0.37,0.39]
12	13	1.4680+j1.1550	60+j35	8	22	2.9	2.5	3	Commercial	10	1.5	[0.39,0.41]
13	14	0.5416+j0.7129	120+j80	18	25	4.2	3.5	8	Residential	220	0.6	[0.41,0.47]
14	15	0.5910+j0.5260	60+j10	10	25	3.2	2.6	5.5	Residential	220	0.5	[0.47,0.51]
15	16	0.7463+j0.5450	60+j20	15	20	2.2	2.6	2	Residential	220	0.5	[0.51,0.52]
16	17	1.2890+j1.7210	60+j20	8	20	2.8	2.8	1.5	Residential	220	0.5	[0.52,0.54]
17	18	0.3720+j0.5740	90+j40	24	20	2.1	2.4	1	Residential	220	0.5	[0.54,0.55]
2	19	0.1640+j0.1565	90+j40	22	25	3.5	3.1	7	Large user	1	1.6	[0.55,0.60]
19	20	1.5042+j1.3554	90+j40	6	22	2.2	2.5	4	Residential	220	0.5	[0.60,0.62]
20	21	0.4095+j0.4784	90+j40	22	26	3.9	3.6	8	Residential	220	0.5	[0.62,0.68]
21	22	0.7089+j0.9373	90+j40	8	22	2.4	2.8	5.5	Residential	220	0.5	[0.68,0.71]
3	23	0.4512+j0.3-83	90+j50	10	23	2.3	2.2	4	Large user	1	1.6	[0.71,0.74]
23	24	0.8980+j0.7091	420+j200	18	26	3.6	3.3	8	Residential	220	0.6	[0.74,0.79]
24	25	0.8960+j0.7011	420+j200	10	24	2.3	2.8	5.5	Residential	220	0.6	[0.79,0.82]
6	26	0.2030+j0.1034	60+j25	6	22	1.2	2.2	4.5	Commercial	10	1.4	[0.82,0.84]
26	27	0.2842+j0.7006	60+j25	5	22	2.1	1.6	4.5	Commercial	10	1.4	[0.84,0.86]
27	28	1.0590+j0.9337	60+j20	8	22	1.8	1.9	4.5	Commercial	10	1.4	[0.86,0.89]
28	29	0.8042+j0.7006	120+j70	14	26	3.4	2.9	7.5	Residential	220	0.6	[0.89,0.94]
29	30	0.5075+j0.2585	200+j600	5	24	2.2	2.4	6	Residential	220	0.6	[0.94,0.97]
30	31	0.9744+j0.9630	150+j70	18	22	1.1	1.5	3	Residential	220	0.6	[0.97,0.98]
31	32	0.3105+j0.3619	210+j100	12	20	1.5	1.4	2.5	Residential	220	0.6	[0.98,0.99]
32	33	0.3410+j0.5362	60+j40	15	20	1.2	1.4	2	Residential	220	0.5	[0.99,1]

2) RESULT OF OPTIMAL ALLOCATION

MOPSO, NSGA-II, and MOIBA are applied to compare the performance for solving the multi-objective optimization problem. And their parameters are set as follows. The number of populations and maximum iteration are 50 and 300, respectively. The maximum and minimum equivalent impedance of CHB-FCL are 10 and 0, respectively. The maximum and minimum number of CHB-FCL are 8 and 1, respectively. The pre-set phase is 10. The penalty coefficient is 100. The permissible limit current is 12kA. The maximum and minimum influencing factors of SIW are 0.9 and 0.4, respectively. The maximum and minimum frequency of bats are 1 and 0, respectively. The iteration parameter is 2.3. The maximum and minimum loudness of bats are 0.9 and 0.6, respectively.

At present, few works of literature have conducted experimental verification on the life of CHB-FCL. In order to calculate the relationship between the loss coefficient and the current,  $S_{Qmin}$ ,  $S_{Qmax}$ ,  $I_{act}$ , and  $I_{max}$  are set as 0.0001, 0.01, 5kA, 30kA, respectively. Further, CHB-FCL has not been fully commercialized and lacks specific cost parameters, references usually set the cost of the current-limiting reactor supporting facilities to be 5-10 times the installation cost. The capacity cost is selected as the benchmark cost, and the ratio of installation cost  $c_p$  and capacity cost  $c_r$  of CHB-FCL is set as 1: 0.1. The coefficient of price change  $q$  is 0.01. The rate of inflation  $b$  is 0.03. The interest rate  $p$  is 0.06. The operation cost factor  $k_{co}$  is 0.04. The annual maintenance cost factor  $k_{cf}$  is 0.4. The failure rate function parameters  $\alpha_1$ ,  $\alpha_2$  and  $\beta_1$ ,  $\beta_2$  are 0.2, 0.4, 1.74, and 10.32, respectively. The disposal cost

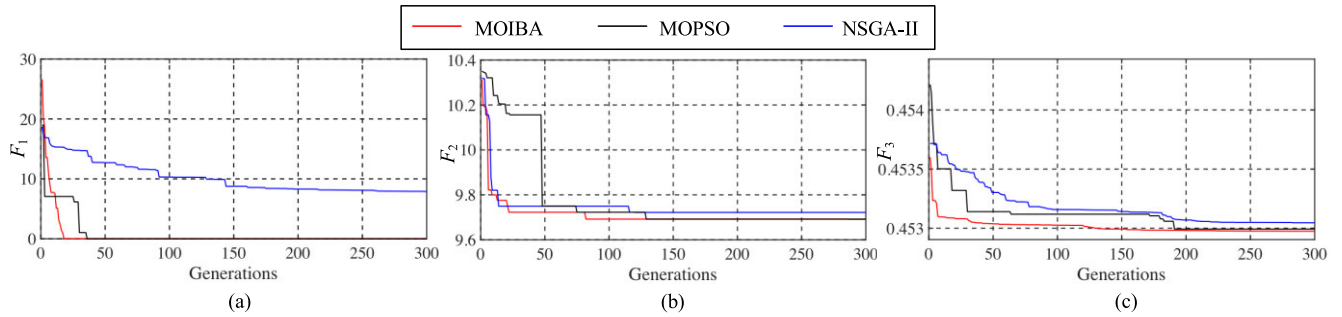


FIGURE 10. The convergence property for objective functions of MOIBA and other methods (a) The first objective function (b) The second objective function (c) The third objective function.

TABLE 3. Fault currents and candidate branches to install the CHB-FCLs.

Node number	Fault current (kA)	Ranking of candidate branches based on sensitivity analysis
5	10.6440	6-26(1.9353), 5-6(1.8741), 29-30(0.9696), 30-31(0.9342), 31-32(0.8971), 32-33(0.8946)
6	14.1514	3-23(1.2805), 6-26(1.0085), 32-33(0.9433), 31-32(0.9254), 20-21(0.9214), 19-20(0.9176)
7	12.1318	6-26(5.3511), 3-23(1.5641), 32-33(0.9361), 31-32(0.9359), 24-25(0.9158), 30-31(0.9020)
26	12.5335	3-23(1.3934), 24-25(0.9461), 9-10(0.9453), 20-21(0.9284), 21-22(0.9200), 19-20(0.9118)
27	10.6252	3-23(1.5288), 6-26(1.5036), 24-25(0.9615), 9-10(0.9449), 19-20(0.9242), 1-2(0.9195)

TABLE 4. Candidate locations of CHB-FCLs with sensitivity factor analysis.

Candidate locations	The sensitivity factor $\eta \times 10^5$	Candidate locations	The sensitivity factor $\eta \times 10^5$
24-25	2.1793	28-29	1.2876
3-4	2.1491	20-21	0.9129
32-33	1.7190	13-14	0.8557
31-32	1.3172	26-27	0.8451

factor  $k_{cd}$  is 0.1. The research phase  $t_r$  is 50 years. The repair time of the bus and line are 2 and 5, respectively.

The convergence curves of objective functions are depicted in Fig. 10. It can be seen from Fig. 10 that the MOIBA's convergence curves have a sharp decline in the first 50 iterations and reach the minimum value before 150 iterations. It can be affirmed that MOIBA has quicker convergence speed and better search accuracy than MOPSO and NSGA-II because it can jump out of local extremum easily and determined the globally optimal values.

Fig. 11 shows the Pareto front with the unfixed number of CHB-FCLs obtained from MOIBA, MOPSO, and NSGA-II, and the three curves are depicted in one figure. From Figure 11, it can be obtained that the Pareto front set of the MOIBA algorithm is dominated in those of the other two methods. Among them, the distribution of the results

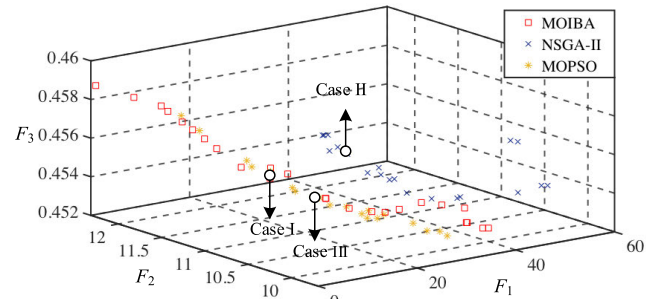


FIGURE 11. All used algorithms Pareto front for IEEE 33-bus system.

TABLE 5. Optimization solutions of the selected three cases.

Item	Scheme	Service life $t_{FCL}$	Mitigation effect	WLRI	LCC
Case I (MOIBA)	3-4 (1.0495)	11	10.7294	0.4557	948.564
	20-21 (1.4219)	10			
	28-29 (2.9521)	6			
Case II (NSGA-II)	3-4 (2.8008)	15	10.8008	0.4573	1460.3
	20-21 (3.8287)	10			
	24-25 (1.1829)	10			
	31-32 (0.9485)	10			
Case III (MOPSO)	32-33 (6.5646)	10			
	13-14 (0.3793)	10	10.9040	0.4561	955.655
	26-27 (0.3297)	10			
	28-29 (4.0766)	6			

obtained by NSGA-II is relatively concentrated and scattered, which is caused by the local optimal solution being trapped in the search process and not jumping out of the search range. In contrast, MOIBA and MOPSO have a wide range of solutions. Due to the use of a novel crowding distance, the distribution of MOIBA's solutions more uniform than MOPSO. Although the solution sets obtained by the algorithm are different, all the Pareto optimal solutions obtained by the same algorithm are equal and are considered as an optimal solution.

Table 5 shows three typical solutions and corresponding parameters are selected from the Pareto Front.

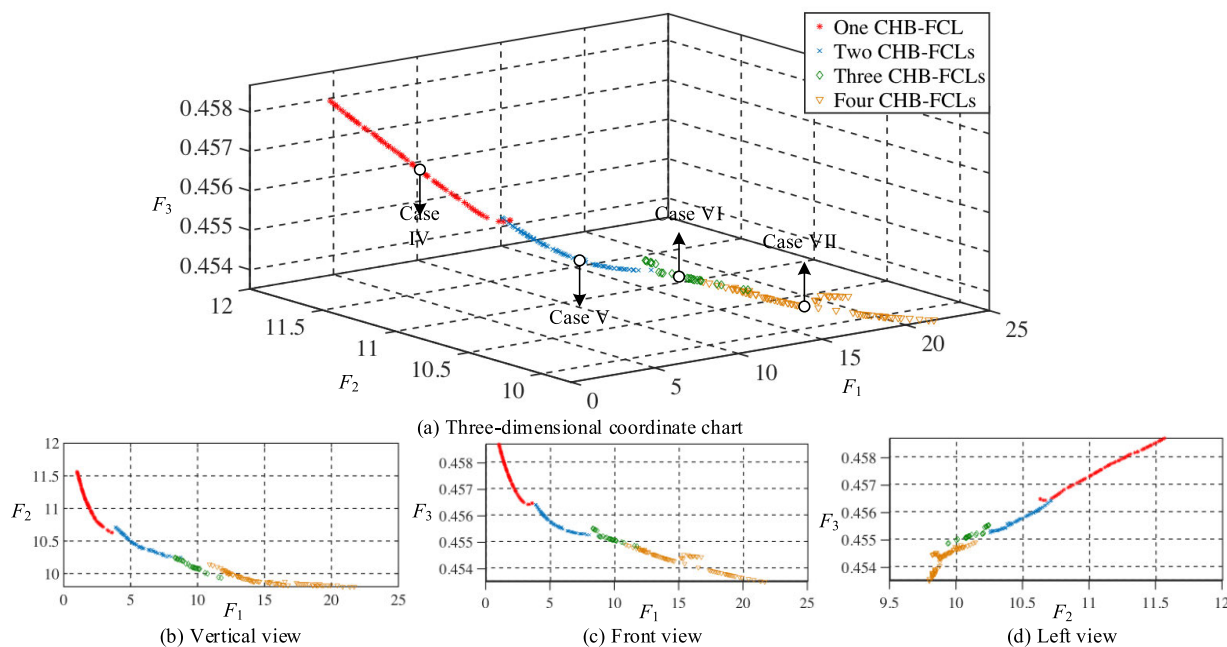


FIGURE 12. Pareto front features of optimal allocation of CHB-FCLs using MOIBA algorithm.

TABLE 6. Optimal solutions of the selected four cases.

Item	Location	Impedances OF CHB-FCLs	Service life $t_{FCL}$	Objective function $F_1$	Objective function $F_2$	Objective function $F_3$	LCC	CI	CO	CF	CD
Case IV	28-29	0.6117	10	1.6117	11.1416	0.4577	288.683	181.344	55.978	39.679	11.682
Case V	28-29	2.0247	10	5.5445	10.4201	0.4556	572.604	355.603	113.967	80.584	22.450
	3-4	1.5198	15								
Case VI	28-29	5.5825	5	10.7405	10.0002	0.4550	993.627	651.667	173.051	123.618	45.291
	3-4	1.7492	15								
	26-27	0.4088	13								
Case VII	28-29	4.5262	6	15.9536	9.8597	0.4545	1440.4	970.184	232.149	167.671	70.359
	3-4	2.9731	6								
	26-27	0.7945	10								
	13-14	3.6598	10								

As can be seen from the table, the scheme selected by NSGA-II is equipped with five CHB-FCLs, the scheme selected by MOPSO is equipped with three CHB-FCLs and the scheme selected by MOIBA is equipped with three CHB-FCLs. And the installation positions of MOIBA partially overlap with case II and case III. The results are obtained by MOIBA, which have more reduction in the three objective functions when it is compared to the other algorithms. However, the current flowing through the limiter is more massive with the smaller number of CHB-FCLs, resulting in more loss life of the limiter, and the cost is increased due to the shortened service life. In summary, MOIBA not merely has a faster convergence rate but also achieves a better Pareto front solution set. It is worth mentioning that the multi-objective optimization algorithm is to minimize all objective functions. There is no one solution to minimize

all objective functions and the reduction of one objective function will inevitably lead to an increase in other objective functions. Therefore, the complete solution set makes it easier for decision-makers to choose.

Fig. 12 shows the Pareto front of CHB-FCLs using MOIBA. The three axes represent the three objective functions, and the red, blue, green, and yellow curves represent the Pareto optimal solutions when there are 1, 2, 3, and 4 CHB-FCLs, respectively. It can be seen from Fig. 11, the objective function of the capital cost is inversely proportional to mitigation current effect and the reliability. As well as the objective functions of the mitigation effect is proportional to reliability. If the capital cost is less, the current mitigation effect and the reliability are worse. The better the reliability required, the higher the current mitigation effect.

**TABLE 7.** The simulation parameters of the fault line model and customer data in the IEEE 30-bus system.

From $i$	To $j$	Impedance $r+jx(\Omega)$	Susceptance (S)	$X_1$	$X_2$	$X_3$	$X_4$	$X_5$	Type	Number of Customers	$\omega_k$	$[P_1, P_2]$
1	2	0.02+j0.06	0.03	30	30	1.2	2.4	10	Large user	1	1.8	[0,0.0468]
1	3	0.05+j0.19	0.02	10	28	2.8	3.9	7	Commercial	10	1.5	[0.0468,0.0874]
2	4	0.06+j0.17	0.02	9	25	3.0	3.2	6.8	Commercial	10	1.5	[0.0874,0.1232]
3	4	0.01+j0.04	0	8	20	3.3	3.5	4	Residential	220	0.5	[0.1232,0.1459]
2	5	0.05+j0.2	0.02	12	25	3.2	3.1	7.5	Large user	1	1.6	[0.1459,0.1847]
2	6	0.06+j0.18	0.02	24	22	2.7	3.0	6.5	Commercial	10	1.5	[0.1847,0.2167]
4	6	0.01+j0.04	0	18	22	2.5	3.9	3.2	Commercial	10	1.5	[0.2167,0.2384]
5	7	0.05+j0.12	0	15	23	2.8	2.5	9.1	Large user	1	1.7	[0.2384,0.2785]
6	7	0.03+j0.08	0	18	20	3.0	1.3	6.0	Residential	220	0.6	[0.2785,0.3029]
6	8	0.01+j0.04	0	20	22	2.6	2.6	6.8	Commercial	10	1.5	[0.3029,0.3343]
6	9	0+j0.21	0	19	26	2.3	2.0	7.8	Commercial	10	1.5	[0.334,0.3706]
6	10	0+j0.56	0	28	22	2.9	2.5	8.2	Commercial	10	1.5	[0.3706,0.4082]
9	11	0+j0.21	0	8	25	4.2	3.5	10	Large user	1	1.6	[0.4082,0.4591]
9	10	0+j0.11	0	10	25	3.2	2.6	7.8	Residential	220	0.5	[0.4591,0.4975]
4	12	0+j0.26	0	15	20	2.2	2.6	6	Residential	220	0.5	[0.4975,0.5226]
12	13	0+j0.14	0	8	20	2.8	2.8	9.5	Large user	1	1.6	[0.5226,0.5612]
12	14	0.12+j0.26	0	14	20	2.1	2.4	8.3	Residential	220	0.5	[0.5612,0.5933]
12	15	0.07+j0.13	0	10	25	3.5	3.1	5	Residential	220	0.5	[0.5933,0.6242]
12	16	0.09+j0.2	0	28	22	2.2	2.5	3.4	Residential	220	0.5	[0.6242,0.6432]
14	15	0.22+j0.2	0	18	26	3.9	3.6	4	Residential	220	0.5	[0.6432,0.6747]
16	17	0.08+j0.19	0	8	22	2.4	2.8	2.2	Residential	220	0.5	[0.6747,0.6889]
15	18	0.11+j0.22	0	16	23	2.3	2.2	3	Residential	220	0.6	[0.6889,0.7058]
18	19	0.06+j0.13	0	18	26	3.6	3.3	2.1	Residential	220	0.6	[0.7058,0.7292]
19	20	0.03+j0.07	0	10	24	2.3	2.8	2	Residential	220	0.6	[0.7292,0.7445]
10	20	0.09+j0.21	0	22	22	1.2	2.2	3	Commercial	10	1.4	[0.7445,0.7580]
10	17	0.03+j0.08	0	6	22	2.1	1.6	3.7	Commercial	10	1.4	[0.7580,0.7735]
10	21	0.03+j0.07	0	16	22	1.8	1.9	3.5	Commercial	10	1.4	[0.7735,0.7891]
10	22	0.07+j0.15	0	8	26	3.4	2.9	2.3	Residential	220	0.6	[0.7891,0.8105]
21	22	0.01+j0.02	0	5	24	2.2	2.4	1.9	Residential	220	0.6	[0.8105,0.8238]
15	23	0.1+j0.2	0	23	22	1.1	1.5	2.3	Residential	220	0.6	[0.8238,0.8330]
22	24	0.12+j0.18	0	12	20	1.5	1.4	1.8	Residential	220	0.6	[0.8330,0.8383]
23	24	0.13+j0.27	0	34	20	1.2	1.4	1.5	Residential	220	0.5	[0.8383,0.8439]
24	25	0.19+j0.33	0	12	20	2.8	2.2	1.4	Residential	220	0.5	[0.8439,0.8535]
25	26	0.25+j0.38	0	5	28	2.5	1.9	1.2	Residential	220	0.5	[0.8535,0.8678]
25	27	0.11+j0.21	0	25	24	2.8	2.9	1.4	Residential	220	0.5	[0.8678,0.8842]
28	27	0+j0.4	0	16	29	2.2	1.1	3.8	Commercial	10	1.4	[0.8842,0.9068]
27	29	0.22+j0.42	0	10	20	1.2	1.8	1.1	Commercial	10	1.4	[0.9068,0.9097]
27	30	0.32+j0.6	0	10	20	1.2	1.8	1.1	Commercial	10	1.4	[0.9097,0.9125]
29	30	0.24+j0.45	0	16	25	2.6	2.2	1.0	Residential	220	0.5	[0.9125,0.9254]
8	28	0.06+j0.2	0.02	14	22	2.6	3.6	7.7	Large user	1	1.6	[0.9254,0.9617]
6	28	0.02+j0.06	0.02	20	28	2.8	2.4	7.1	Commercial	10	1.4	[0.9617,1]

Four cases are selected and marked as Case IV, Case V, Case VI, and Case VII, which represent four optimized solutions of the CHB-FCLs, and the detailed optimization data are listed in Table 6. These results show the optimal choice with a different preference for the objective. If the objective function

of  $F_1$  is subject to  $0 < F_1 < 3.8$ , installing one CHB-FCL is optimal. If  $9.78 < F_2 < 10.23$  and  $0.453 < F_3 < 0.455$ , installing four CHB-FCLs is optimal. Moreover, installing two or three CHB-FCLs are the tradeoff of the three objective functions. In the 50-year life cycle cost, the investment cost

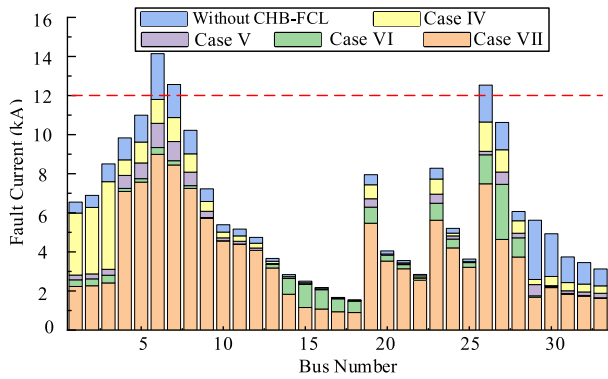


FIGURE 13. Bus fault currents of IEEE 33-bus distribution system.

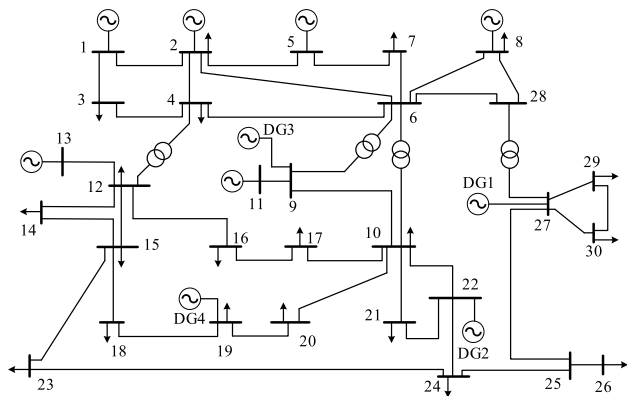


FIGURE 14. Schematic of the modified IEEE 33-bus system with DGs.

of the CHB-FCLs accounts for 60% of the main expenditure, the operation cost, and maintenance cost account for about 20% and 10%, and the rest is the recovery cost.

Fig. 13 shows the bus fault currents with different cases. There are three buses (6,7, and 26) with excessive fault current and the fault current increases significantly near the head end of the feeder and the DGs. In all schemes, the fault current of each node falls below the permissible limit current  $I_{per}^{max}$ , in which the current limiting effect of Case VII is the best, and the current limiting effect of Case IV is the worst. With the increase in the number of CHB-FCLs, the mitigation effect and WLRI of CHB-FCL can be improved, but the cost may increase. Therefore, the selection of the optimal solution depends on the subjective judgment of the decision-maker.

**B. IEEE 30-BUS SYSTEM WITH DGs**

Fig. 14 shows the IEEE 30-bus Benchmark system, which consists of 30 nodes,10 generators, 12 transformers and 34 lines. And Table 7 gives the simulation parameters. The base voltage is 135kV, the base capacity of the system is 100MVA. Combining [24] and system load capacity, four 500kVA photovoltaic plants (marked as DG1, DG2, DG3, and DG4) are installed at bus 27, 22, 9, and 19, respectively. And the subtransient reactance  $Z_{DG}$  is 0.2. The threshold of exceeding current is set as 13 pu.

TABLE 8. Fault currents and candidate branches to install the CHB-FCLs.

Node number	Fault current (pu.)	Ranking of candidate branches based on sensitivity analysis $\eta * 10^4$
4	17.5486	21-22(39.688), 10-21(5.863), 29-30(5.451), 10-22(1.492), 25-26(1.297), 23-24(0.935)
6	26.3140	21-22(197.7), 19-20(154.8), 16-17(950.3), 18-19(8.494), 10-22(6.740), 10-20(5.913)
8	15.2264	19-20(144.5), 29-30(28.015), 16-17(18.83), 23-24(14.234), 18-19(11.695), 10-17(0.657)
10	17.7466	29-30(198.53), 27-29(0.651), 27-30(0.635), 25-27(0.324), 25-26(0.215), 1-2(0.055)
21	17.7466	3-4(34.095), 1-3(18.189), 1-2(13.653), 5-7(6.815), 2-4(4.609), 2-5(3.241)
22	13.7661	2-5(109.12), 5-7(856.61), 1-2(568.49), 6-7(133.80), 4-6(35.252), 3-4(30.709)
28	14.0843	18-19(723.4), 19-20(106.0), 15-18(29.180), 16-17(20.034), 10-17(6.940), 10-20(4.168)

TABLE 9. Candidate locations of CHB-FCLs with sensitivity factor analysis.

Candidate locations	The sensitivity factor $\eta * 10^9$	Candidate locations	The sensitivity factor $\eta * 10^9$
29-30	12.024	2-5	0.4504
21-22	10.859	27-29	0.3984
9-11	4.4092	27-30	0.3965
19-20	0.5375	10-22	0.3893

1) SELECTING CANDIDATE LOCATIONS

In the traditional sensitivity analysis model, seven fault current nodes and their candidate branches are given in Table 8. By selecting the repetitive locations and sorting the locations at the front, CHB-FCLs are installed in eight candidate branches, namely, 1-2, 2-5, 3-4, 16-17, 18-19, 19-20, 21-22, and 29-30. However, the traditional sensitivity analysis model leads to unnecessary planning, such as continuous placement of adjacent lines and failure to consider the importance of branches.

In the proposed sensitivity factor analysis, the candidate positions of the fault current limiter are listed in Table 9.

It can be seen from Table 9, the top eight branches of the total value of sensitivity factors are selected as candidate locations, namely, 2-5, 9-11, 10-22, 19-20, 21-22, 27-19, 27-30, 29-30. The schemes are overlapped with those of the traditional sensitivity analysis model and installed near DGs.

2) RESULT OF OPTIMAL ALLOCATION

Fig. 15 illustrates the convergence curves of objective functions. It can be seen that MOIBA’s convergence curve reaches the minimum value before 100 iterations. It can be affirmed that MOIBA has a quicker convergence speed and better search accuracy than MOPSO and NSGA-II.

Fig. 16 represents the Pareto front obtained by MOIBA, MOPSO, and NSGA-II for the IEEE 30-bus Benchmark system, and the Pareto front obtained from these methods are depicted in one figure. The results obtained by MOIBA dominate the results obtained by the other two methods. However, the obtained solution set is subject to the mutual

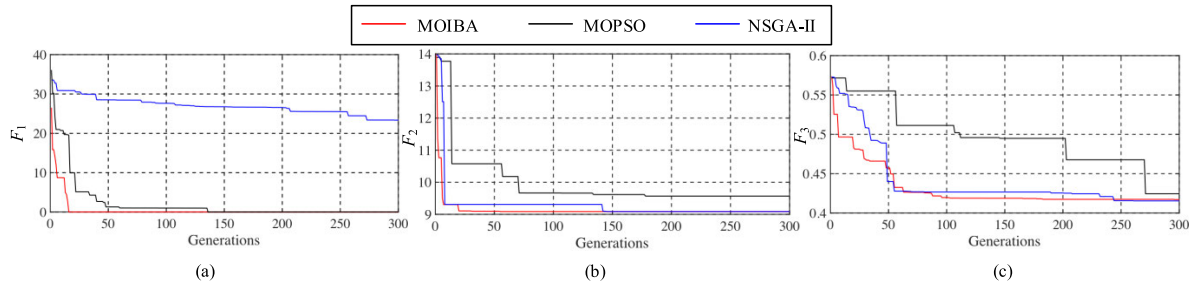


FIGURE 15. The convergence property for objective functions of MOIBA and other methods (a) The first objective function (b) The second objective function (c) The third objective function.

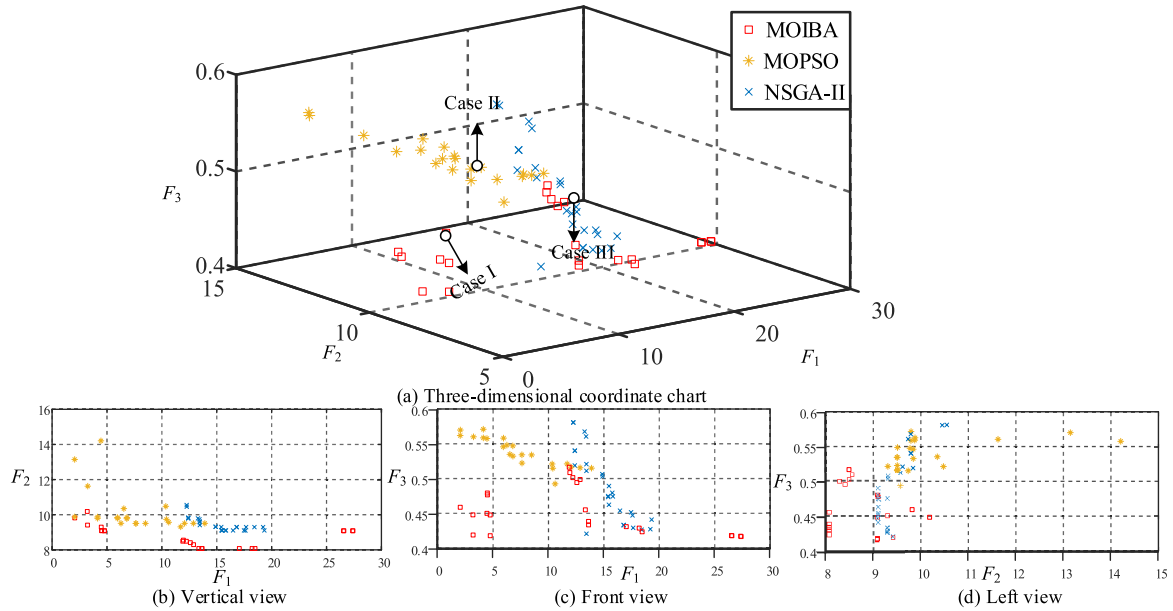


FIGURE 16. Pareto front features of optimal allocation of CHB-FCLs using MOIBA algorithm.

TABLE 10. Optimal solutions of the selected four cases.

Item	Location	Impedances Of CHB-FCLs	Service life $t_{FCL}$	Objective function $F_1$	Objective function $F_2$	Objective function $F_3$	LCC	CI	CO	CF	CD
Case I	9-11	2.0507	10	8.3448	9.4969	0.4326	1163	730.43	225.56	159.88	47.07
	19-20	0.0303	10								
	21-22	2.1603	10								
	27-29	0.1035	10								
Case II	9-11	0.0136	10	7.4115	9.5678	0.5196	1425	891.50	279.33	197.36	56.94
	19-20	0.2585	10								
	10-22	0.1280	14								
	21-22	1.4398	10								
Case III	9-11	0.0133	10	6.4269	9.5015	0.4879	1421	888.91	278.52	196.78	56.76
	19-20	0.5629	10								
	10-22	0.4557	14								
	27-29	0.4257	10								
	29-30	0.0154	10								

constraints between the objective functions, so that each solution in the solution set is a feasible solution. From the Pareto

fronts obtained by MOIBA, MOPSO, and NSGA-II, three typical solutions are selected and marked as Case I, Case II,

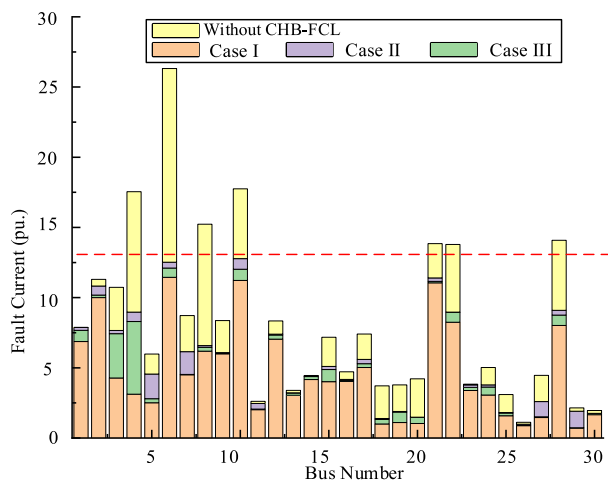


FIGURE 17. Bus fault currents of IEEE 30-bus distribution system.

and Case III to describe the specific parameters of each scheme.

As can be seen from Table 10, the scheme selected by MOPSO and NSGA-II are equipped with five CHB-FCLs, and the scheme selected by MOIBA is equipped with four CHB-FCLs. Although the objective function  $F_1$  of Case I is high, the current limiting effect and reliability of this scheme are better than other cases. The fewer number of CHB-FCLs make the LCC of Case I smaller than other cases. In the 50-year life cycle cost, the investment cost of the CHB-FCLs accounts for 60% of the main expenditure, the operation cost, and maintenance cost account for about 20% and 10%, and the rest is the recovery cost.

In order to directly reflect the current limiting effect of each case, Fig. 17 shows the fault currents with different cases. When the CHB-FCL is not installed, there are seven buses (4, 6, 8, 10, 21, 22, and 28) with excessive fault current. In all schemes, the fault current of each node falls below the threshold of exceeding current, in which the current limiting effect of Case I is the best, and the current limiting effect of Case III is the worst.

## VI. CONCLUSION

In order to give full play to the CHB-FCL's flexible adjustable ability, this paper proposes a novel methodology. The novel methodology consists of the sensitivity factor analysis, a multi-objective improved bat algorithm, and the economic evaluation model. Considering the three objectives of the cost of CHB-FCLs, the mitigation effect and WLRI, the proposed approach is verified by the modified IEEE 33-bus system and IEEE Benchmark system. The significant contributions of this study can be summarized as follows:

(i) Based on the Monte Carlo fault simulation model, the sensitivity factor analysis method is proposed to rank candidate locations, which is not only closer to the actual situation of the network than the traditional sensitivity analysis, but also improves the search space and speed of multi-objective optimization problems.

(ii) SIWstrategy, ILS strategy, balance strategy and non-dominant sorting strategy are introduced into the standard bat algorithm. And the proposed multi-objective improved bat algorithm is applied to search the Pareto front solution set, which has better convergence precision and spatial distribution than NSGA2 and MOPSO.

(iii) The economic evaluation model is proposed, which is used to calculate the service life of the CHB-FCL considering the operating loss and calculated the NPV of all kinds of costs in the research phase.

Compared with the previous optimal configuration method, the proposed method not only has higher accuracy and a better Pareto front solution set, but also entirely constructs the economic model of CHB-FCLs. All in all, the proposed method provides a good idea for the optimal configuration of the CHB-FCLs and feasible suggestions for engineering planning.

## REFERENCES

- [1] W. T. B. de Sousa, D. Kottonau, S. Karrari, J. Geisbusch, and M. Noe, "Deployment of a resistive superconducting fault current limiter for improvement of voltage quality and transient recovery voltage," *IEEE Trans. Appl. Supercond.*, vol. 31, no. 1, pp. 1–9, Jan. 2021.
- [2] M. Aurangzeb, A. Xin, S. Iqbal, and M. U. Jan, "An evaluation of flux-coupling type SFCL placement in hybrid grid system based on power quality risk index," *IEEE Access*, vol. 8, pp. 98800–98809, May 2020.
- [3] Y. Kim, H.-C. Jo, and S.-K. Joo, "Analysis of impacts of superconducting fault current limiter (SFCL) placement on distributed generation (DG) expansion," *IEEE Trans. Appl. Supercond.*, vol. 26, no. 4, pp. 1–5, Jun. 2016.
- [4] F. Zheng, C. Deng, L. Chen, S. Li, Y. Liu, and Y. Liao, "Transient performance improvement of microgrid by a resistive superconducting fault current limiter," *IEEE Trans. Appl. Supercond.*, vol. 25, no. 3, pp. 1–5, Jun. 2015.
- [5] C. Guo, C. Ye, Y. Ding, Z. Lin, and P. Wang, "Risk-based many-objective configuration of power system fault current limiters utilising NSGA-III," *IET Gener., Transmiss. Distrib.*, vol. 14, no. 23, pp. 5646–5654, Dec. 2020.
- [6] M. A. Hosseinzadeh, M. Sarbanzadeh, A. Salehi, M. Rivera, J. Munoz, and P. Wheeler, "Performance evaluation of cascaded H-bridge multilevel grid-connected converter with model predictive control technique," in *Proc. IEEE Int. Conf. Ind. Technol. (ICIT)*, Melbourne, VIC, Australia, Feb. 2019, pp. 1806–1811.
- [7] E. Loukarakis and G. Stavrakakis, "Adaptive enumeration method for the optimal interconnection planning of isolated power systems," *IET Gener., Transmiss. Distrib.*, vol. 7, no. 3, pp. 235–243, Mar. 2013.
- [8] P. Yu, B. Venkatesh, A. Yazdani, and B. N. Singh, "Optimal location and sizing of fault current limiters in mesh networks using iterative mixed integer nonlinear programming," *IEEE Trans. Power Syst.*, vol. 31, no. 6, pp. 4776–4783, Nov. 2016.
- [9] H. Zeineldin, E. El-Saadany, and L. Huchel, "Protection coordination index enhancement considering multiple DG locations using FCL," in *Proc. IEEE Power Energy Soc. Gen. Meeting*, Chicago, IL, USA, Jul. 2017, p. 1.
- [10] H. B. Habil, E. Azad-Farsani, and H. A. Abyaneh, "A novel method for optimum fault current limiter placement using particle swarm optimization algorithm," *Int. Trans. Electr. Energy Syst.*, vol. 25, no. 10, pp. 2124–2132, Oct. 2015.
- [11] H.-T. Yang, W.-J. Tang, and P. R. Lubicki, "Placement of fault current limiters in a power system through a two-stage optimization approach," *IEEE Trans. Power Syst.*, vol. 33, no. 1, pp. 131–140, Jan. 2018.
- [12] A. Esmaeili, S. Esmaeili, and H. Hojabri, "Short-circuit level control through a multi-objective feeder reconfiguration using fault current limiters in the presence of distributed generations," *IET Gener., Transmiss. Distrib.*, vol. 10, no. 14, pp. 3458–3469, Nov. 2016.
- [13] S. Ghaemi, M. Nazari-Heris, and M. Abapour, "Reliability impact analysis of fault current limiters of distribution network under protection miscoordination due to distributed generations," *Iranian J. Sci. Technol., Trans. Electr. Eng.*, pp. 1–12, Jul. 2020, doi: 10.1007/s40998-020-00365-x.



- [14] L. Chen, X. Zhang, H. Chen, G. Li, J. Yang, X. Tian, Y. Xu, L. Ren, and Y. Tang, "Pareto optimal allocation of resistive-type fault current limiters in active distribution networks with inverter-interfaced and synchronous distributed generators," *Energy Sci. Eng.*, vol. 7, no. 6, pp. 2554–2571, Aug. 2019.
- [15] A. Mahmoudian, M. R. Islam, A. Z. Kouzani, and M. A. P. Mahmud, "Optimal allocation of fault current limiter in distribution network with NSGA-II algorithm," in *Proc. IEEE Int. Conf. Appl. Supercond. Electromagn. Devices (ASEMD)*, Tianjin, China, Oct. 2020, pp. 1–2.
- [16] A. Mahmoudian, M. Niasati, and M. A. Khanesar, "Multi objective optimal allocation of fault current limiters in power system," *Int. J. Electr. Power Energy Syst.*, vol. 85, pp. 1–11, Jun. 2017.
- [17] M. Y. Shih, A. Conde, C. Ángeles-Camacho, E. Fernández, Z. Leonowicz, F. Lezama, and J. Chan, "A two stage fault current limiter and directional overcurrent relay optimization for adaptive protection resetting using differential evolution multi-objective algorithm in presence of distributed generation," *Electr. Power Syst. Res.*, vol. 190, Jan. 2021, Art. no. 106844.
- [18] M. Esmaili, M. Ghamsari-Yazdel, N. Amjadi, and C. Y. Chung, "Optimal placement of resistive/inductive SFCLs considering short-circuit levels using complex artificial bee colony algorithm," *IET Gener., Transmiss. Distrib.*, vol. 13, no. 24, pp. 5561–5568, Dec. 2019.
- [19] J. Teng and C. Lu, "Optimum fault current limiter placement with search space reduction technique," *IET Gener., Transmiss. Distrib.*, vol. 4, no. 4, pp. 485–494, Apr. 2010.
- [20] P. T. Ngoc and J. G. Singh, "Short circuit current level reduction in power system by optimal placement of fault current limiter," *Int. Trans. Electr. Energy Syst.*, vol. 27, no. 12, Nov. 2017.
- [21] M. F. Guo, L. X. You, and X. Y. Wei, "A flexible current limiting method of distribution network short circuit fault based on the voltage feedback control," *Trans. China Electrotechn. Soc.*, vol. 32, no. 11, pp. 48–56, Jun. 2017.
- [22] G. Mohapatra, "Current control of a PV integrated CHB-multilevel inverter using PR controller," in *Proc. Technol. Smart-City Energy Secur. Power (ICSESP)*, Bhubaneswar, India, Mar. 2018, pp. 1–6.
- [23] F. Khalilzadeh Moghaddam and H. Iman-Eini, "Reliable simple method for suppression of leakage current in grid-connected CHB inverters," *IET Power Electron.*, vol. 11, no. 13, pp. 2170–2177, Nov. 2018.
- [24] Y. Q. Peng, X. N. Lin, L. Chen, Z. T. Li, X. Ma, and Z. X. Wang, "Research on global cooperative configuration of superconducting fault current limiter considering life cycle cost," *CSEE J. Power Energy Syst.*, vol. 39, no. 21, pp. 6275–6287, Nov. 2019.
- [25] Z. Zeng and Q. Gong, "Fuzzy comprehensive evaluation of security maintenance ability base on AHP-entropy," in *Proc. 3rd Int. Conf. Circuits, Syst. Simulation (ICCSS)*, Nanjing, China, Jun. 2019, pp. 166–171.
- [26] S.-Y. Kim, W.-W. Kim, and J.-O. Kim, "Determining the location of superconducting fault current limiter considering distribution reliability," *IET Generat. Transmiss. Distrib.*, vol. 6, no. 3, pp. 240–246, Mar. 2012.
- [27] G. Chen, J. Qian, Z. Zhang, and Z. Sun, "Applications of novel hybrid bat algorithm with constrained Pareto fuzzy dominant rule on multi-objective optimal power flow problems," *IEEE Access*, vol. 7, pp. 52060–52084, Apr. 2019.
- [28] G. Chen, J. Qian, Z. Zhang, and Z. Sun, "Multi-objective optimal power flow based on hybrid firefly-bat algorithm and constraints-prior object-fuzzy sorting strategy," *IEEE Access*, vol. 7, pp. 139726–139745, Sep. 2019.
- [29] C. Gan, W. Cao, M. Wu, and X. Chen, "A new bat algorithm based on iterative local search and stochastic inertia weight," *Expert Syst. Appl.*, vol. 104, pp. 202–212, Aug. 2018.
- [30] Z. He, J. Zhou, L. Mo, H. Qin, X. Xiao, B. Jia, and C. Wang, "Multi-objective reservoir operation optimization using improved multiobjective dynamic programming based on reference lines," *IEEE Access*, vol. 7, pp. 103473–103484, Jul. 2019.
- [31] Y. Sun, G. G. Yen, and Z. Yi, "IGD indicator-based evolutionary algorithm for many-objective optimization problems," *IEEE Trans. Evol. Comput.*, vol. 23, no. 2, pp. 173–187, Apr. 2019.
- [32] W. Hu, G. G. Yen, and X. Zhang, "Multiobjective particle swarm optimization based on Pareto entropy," *Software*, vol. 25, no. 5, pp. 1025–1050, 2014.
- [33] N. B. Abdul Rahim and T. L. J. Ferris, "A method to establish a trade-space of system requirements and life cycle cost," *IEEE Syst. J.*, vol. 14, no. 1, pp. 1257–1264, Mar. 2020.
- [34] W. Lai, M. Chen, L. Ran, O. Alatise, S. Xu, and P. Mawby, "Low stress cycle effect in IGBT power module die-attach lifetime modeling," *IEEE Trans. Power Electron.*, vol. 31, no. 9, pp. 6575–6585, Sep. 2016.
- [35] V. Smet, F. Forest, J.-J. Huselstein, F. Richardeau, Z. Khatir, S. Lefebvre, and M. Berkani, "Ageing and failure modes of IGBT modules in high-temperature power cycling," *IEEE Trans. Ind. Electron.*, vol. 58, no. 10, pp. 4931–4941, Oct. 2011.
- [36] U.-M. Choi, K. Ma, and F. Blaabjerg, "Validation of lifetime prediction of IGBT modules based on linear damage accumulation by means of superimposed power cycling tests," *IEEE Trans. Ind. Electron.*, vol. 65, no. 4, pp. 3520–3529, Apr. 2018.



**ZHENG YU SHU** was born in Yichang, Hubei, China, in 1983. He received the B.S., M.S., and Ph.D. degrees in electric engineering from Wuhan University, China, in 2005, 2009, and 2013, respectively. He is currently a Lecturer with the School of Electrical Engineering and Automation, Three Gorges University. His main research interests include renewable energy fault ride through, and microgrid operation and control.



**YIQIANG CHEN** was born in Quanzhou, Fujian, China, in October 1995. He received the B.S. degree from Fuzhou University, China, in 2018, where he is currently pursuing the M.S. degree. His research interests include current limiter configuration optimization, and microgrid operation and control.



**CHANGHONG DENG** received the Ph.D. degree from the School of Electrical Engineering, Wuhan University, Wuhan, China, in 2007. She is currently a Professor with Wuhan University. Her research interests include power system security and stability analysis, optimal control theory, and renewable energy integration.



**FENG ZHENG** was born in Wenzhou, Zhejiang, China, in 1983. He received the B.S. and M.S. degrees in electric engineering from Three Gorges University, China, in 2006 and 2009, respectively, and the Ph.D. degree in electric engineering from Wuhan University, China, in 2017. He is currently a Lecturer with the School of Electrical Engineering and Automation, Fuzhou University. His main research interests include renewable energy fault ride through, and microgrid operation and control.



**HAO ZHONG** was born in Changde, Hunan, China, in 1983. He received the B.S., M.S., and Ph.D. degrees in electric engineering from Hunan University, China. He is currently a Lecturer with the School of Electrical Engineering and Automation, Three Gorges University. His main research interests include power system operation and control.

• • •